High-Resolution Structure of the HNF-1α Dimerization Domain[†,‡]

Robert B. Rose,[§] James A. Endrizzi,[§] Jeff D. Cronk,[||] James Holton, and Tom Alber*

Department of Molecular and Cell Biology, 229 Stanley Hall #3206, University of California, Berkeley, California 94720-3206

Received August 22, 2000; Revised Manuscript Received October 4, 2000

ABSTRACT: The N-terminal dimerization domain of the transcriptional activator hepatocyte nuclear factor-1α (HNF-1α) is essential for DNA binding and association of the transcriptional coactivator, DCoH (dimerization cofactor of HNF-1). To investigate the basis for dimerization of HNF-1 proteins, we determined the 1.2 Å resolution X-ray crystal structure of the dimerization domain of HNF-1α (HNF-p1). Phasing was facilitated by devising a simple synthesis for Fmoc-selenomethionine and substituting leucine residues with selenomethionine. The HNF-1 dimerization domain forms a unique, four-helix bundle that is preserved with localized conformational shifts in the DCoH complex. In three different crystal forms, HNF-p1 displays subtle shifts in the conformation of the interhelix loop and the crossing angle between the amino- and carboxyl-terminal helices. In all three crystal forms, the HNF-p1 dimers pair through an exposed hydrophobic surface that also forms the binding site for DCoH. Conserved core residues in the dimerization domain of the homologous transcriptional regulator HNF-1β rationalize the functional heterodimerization of the HNF-1α and HNF-1β proteins. Mutations in HNF-1α are associated with maturity-onset diabetes of the young type 3 (MODY3), and the structure of HNF-p1 provides insights into the effects of three MODY3 mutations.

Dimerization is a key determinant of both DNA binding selectivity and biological activity of many transcriptional activators (reviewed in ref *1*). Dimerization generally enhances DNA binding affinity, often restricting DNA recognition to palindromic sequences. In many cases, heterodimerization with paralogs possessing altered dimerization and DNA binding affinities (e.g., fos/jun or mad/max) or activation properties [e.g., c-Jun, Jun-B, and Jun-D (*2*−*4*)] modulates the regulatory activity. Autonomous dimerization domains define several classes of transcription factors, including the leucine−zipper, helix−loop−helix, and helix−loop−helix−zipper families.

The homeodomain proteins HNF-1α[1] and HNF-1β comprise a functionally important family in which dimerization is essential for DNA binding (*5*). HNF-1α and HNF-1β regulate tissue-specific genes in liver, kidney, intestine, and pancreas (*6*, *7*). Mutations in HNF-1α and HNF-1β in humans have been associated with two subtypes of non-insulin-dependent diabetes, maturity-onset diabetes of the young type 3 (MODY3) (*8*) and type 5 (MODY5) (*9*, *10*), respectively. These proteins form homo- and heterodimers through an autonomously folded domain encompassing the 32 N-terminal amino acids (*6*, *11*−*15*). The dimerization domain also binds the transcriptional coactivator DCoH, which stimulates HNF-1α activity (*16*).

Dimerization of HNF-1α and HNF-1β is thought to impart combinatorial diversity to the regulatory responses mediated by these proteins. HNF-1α and HNF-1β share similar dimerization and DNA binding properties, but they possess distinct activation domains (*11*, *14*, *17*, *18*). Like HNF-1α, HNF-1β homodimers activate transcription in vivo (*19*). One isoform of HNF-1β lacks an activation domain, and heterodimerization with HNF-1α inhibits transcription of HNF-1α-dependent genes (*20*). Expression of HNF-1β has been associated with dedifferentiation in cell culture (*14*, *21*−*23*). It has been proposed that the ratio of HNF-1α to HNF-1β correlates with the stage of differentiation in hepatocellular carcinoma (*24*). HNF-1α and HNF-1β monomers exchange readily in vitro to form homo- and heterodimers (*16*). DCoH inhibits subunit exchange by interacting with the dimerization domain.

The isolated HNF-1α dimerization domain forms a stable dimer in solution (*5*) and associates in a 2:2 complex with the coactivator DCoH (*25*). On the basis of circular dichroism (*15*), NMR (*26*, *27*), and sequence homology (*28*), the dimerization domains of HNF-1α and HNF-1β have been predicted to form a coiled coil or a four-helix bundle. To define the basis for HNF-1 dimerization and coactivator recognition, we report here the high-resolution crystal

[†] This work was supported by NIH Grant GM54793 and a grant from the W. M. Keck Foundation (T.A.). R.B.R. was supported by postdoctoral fellowships from the NIH and the Juvenile Diabetes Foundation International.

[‡] Coordinates for wild-type HNF-p1 and the Leu12SeMet and Leu13SeMet mutant proteins were deposited in the RCSB Protein Data Bank under entry codes 1G39, 1GZY, and 1GZZ, respectively.

* To whom correspondence should be addressed. Phone: (510) 642-8758. Fax: (510) 643-9290. E-mail: tom@ucxray6.berkeley.edu.

[§] These authors contributed equally to this work.

[||] Present address: Division of Basic Sciences, Fred Hutchinson Cancer Research Center, 1100 Fairview Ave. North, P.O. Box 19024, Seattle, WA 98109-1024.

[1] Abbreviations: HNF-1, hepatocyte nuclear factor-1; HNF-p1, dimerization domain of HNF-1; DCoH, dimerization cofactor of HNF-1; MODY, maturity-onset diabetes of the young; MAD, multiwavelength anomalous diffraction; rms, root-mean-square; SeMet, selenomethionine; TFA, trifluoroacetic acid; Fmoc, *N*-(9-fluorenylmethoxycarbonyl); NHS, *N*-hydroxysuccinimide; PEG, polyethylene glycol; PDB, Protein Data Bank.

10.1021/bi001996t CCC: $19.00
Published on Web 11/16/2000

structure of the HNF-1α dimerization domain. The crystal structure of HNF-p1, alone and in complex with DCoH (*25*), differs dramatically from the reported solution structure (*26*). HNF-p1 forms a unique, antiparallel four-helix bundle that provides a basis for understanding the specificity of dimer formation by this motif. Comparison with the structure of the HNF-p1−DCoH complex (*25*) reveals local conformational shifts in HNF-p1 associated with DCoH binding.

MATERIALS AND METHODS

Selenomethionine Synthesis. A simple protocol for synthesizing *N*-(9-fluorenylmethoxycarbonyl)selenomethionine (Fmoc-SeMet) was developed. Selenomethionine (0.25 g, Calbiochem) was dissolved in 2 mL of 2 M bis-tris (in water) in a 50 mL polypropylene centrifuge tube. Acetone was added to this solution until the selenomethionine began to precipitate. About 8 mL of a 200 mM solution of *N*-(9-fluorenylmethoxycarbonyloxy)succinimide (Fmoc-NHS, Aldrich) was prepared in acetone. The Fmoc-NHS solution (6.3 mL) was added slowly to the selenomethionine solution under a stream of dry N_2 gas. The pH (monitored with pH paper) was kept between 7 and 8 by adding 2 M bis-tris. Unreacted Fmoc-NHS (precipitate that stuck to the walls of the reaction vessel) was dissolved by adding pure acetone. High concentrations of acetone, however, caused the unreacted selenomethionine to precipitate. This precipitate was distinguishable from Fmoc-NHS because it did not stick to the walls of the tube. Unreacted selenomethionine could be dissolved by the addition of water, but it was found to dissolve in any case as the reaction progressed.

The progress of the reaction was monitored by reversed phase HPLC (solvent A, 0.1% TFA in H_2O; solvent B, 0.1% TFA in acetonitrile; flow rate, 2 mL/min) using a C18 semipreparative column (Vydac, 218TP1010). After injection of a 1 μL sample, an isocratic flow of 2% B for 11 min was followed by a 2% B/min gradient to 100% B. Unreacted selenomethionine eluted from the column at approximately 17 min ($\epsilon_{217} \sim 2000$). Unreacted Fmoc-NHS eluted at 50.4 min ($\epsilon_{266} = 22\,000$). The product, Fmoc-SeMet, eluted at 49.9 min ($\epsilon_{266} = 13\,000$), and it clearly could be resolved from Fmoc-NHS and the two oxidized forms of the product, Fmoc-SeMet-O at 40.5 min and Fmoc-SeMet-O_2 at 47.6 min. The oxidized forms of Fmoc-SeMet were enhanced upon addition of hydrogen peroxide, or transition metal ions, such as iron. In the absence of exposure to metal objects, less than 0.1% of the product was found to be oxidized at the end of this procedure.

Because unreacted selenomethionine is easier to remove from the reaction than unreacted Fmoc-NHS, Fmoc-NHS was added only until a small amount (∼10 μmol) of unreacted selenomethionine remained. The acetone was evaporated under the dry N_2 stream, and the remaining product was precipitated by the addition of 30−40 mL of 2 M HCl. The product formed an oily solid that was pelletted in a clinical centrifuge. Contaminating byproducts were removed by dissolving the product in a minimal volume of acetone and precipitating with 40 mL of 2 M HCl. This precipitation was repeated five times. As assayed by HPLC, the purity of the product increased with each wash, and only a minimal amount of product (∼1−3 μmol) was lost.

Dust and acid were removed from the product for peptide synthesis. Dust was removed by filtering (0.2 μm pore size) an acetone solution of the product, washing the filter with excess acetone, and drying the filtrate under the N_2 stream. To remove the acid, the product was dissolved in a minimal amount of acetone and diluted with 10 mL of a 50:50 mixture of water and acetonitrile. The cloudy solution was frozen in liquid N_2 and lyophilized to dryness in a glass container. The dry powder was used for peptide synthesis.

Peptide Synthesis and Purification. An Applied Biosystems 431A peptide synthesizer employing Fmoc chemistry was used to make three peptides: the wild-type, 32-amino-acid dimerization domain of HNF-1α and two HNF-p1 mutant peptides with leucines at position 12 or 13 replaced with selenomethionine. Peptides were purified by reversed phase HPLC using a C18 column (Vydac). Electrospray mass spectrometry confirmed the amino acid composition of each peptide.

Crystallization, Data Collection, and Refinement. Lyophilized HNF-p1 peptides were dissolved in water at a concentration of 10 mg/mL. Initial crystallization conditions were identified using a sparse matrix approach (Hampton Research). Crystals of the wild-type peptide were grown at room temperature and 4 °C by vapor diffusion from 30% PEG 4000, 100 mM Tris-HCl (pH 8.5), and 0.2 M $LiSO_4$. Distinct crystals of the mutant peptides were grown under similar conditions (24% PEG 4000, 80 mM Tris-HCl (pH 8.5), and 0.16 M $LiSO_4$). The crystals were equilibrated in well solution containing 10% v/v glycerol and frozen in liquid N_2 prior to data collection.

X-ray data were collected from the two selenomethionine-containing peptides at four wavelengths encompassing the Se absorption edge (Table 1). Data were processed and analyzed using the Elves automation package (J. Holton, unpublished results) running the programs Mosflm (*29*), Scala (*30*), SOLVE (*31*), MLPHARE (*32*), Dm (*33*), ARP (*34*), and wARP (*34*). The heavy atoms were located initially with SOLVE and refined with MLPHARE. Experimental phases were calculated with MLPHARE and modified with Dm. An initial model was built using wARP. The molecular model was displayed and modified using the graphics program O (*35*). Refinement was completed with higher-resolution data (Table 2) using TNT (*36*) and CNS (*37*). Noncrystallographic symmetry (NCS) restraints were selectively applied during refinement with CNS. Coordinates were superimposed with the program Gem (available at http://util.ucsf.edu/). Surface area calculations were performed with CNS.

Because no suitable metal derivative of wild-type HNF-p1 could be prepared, the structure was determined by molecular replacement. Molecular replacement was carried out with CNS at 15−4 Å resolution. Calculations were performed in space group $P2_1$ using the four monomers in the asymmetric unit of the Leu12SeMet crystal as the search model. This procedure resulted in good values of the correlation coefficient of the translation search (0.47) and the *R*-factor following rigid body refinement (44% to 3 Å resolution). The molecular model was refined to 1.22 Å resolution using CNS. The refinement indicated that the monomers within each dimer were conformationally similar, and the two dimers in the asymmetric unit were conformationally different. Noncrystallographic symmetry restraints were applied to the monomers within each dimer.

Table 1: Data Collection and Phasing Statistics of MAD Data Sets[a]

	Leu12SeMet				Leu13SeMet		
	λ_1 = 0.95372 Å	λ_2 = 0.97957 Å	λ_3 = 0.9798 Å	λ_4 = 1.07812 Å	λ_1 = 0.95372 Å	λ_2 = 0.97957 Å	λ_3 = 0.9798 Å
space group	$P2_1$				$P2_12_12$		
unit cell	a = 31.2 Å, b = 47.9 Å, c = 40.5 Å, β = 93.6°				a = 37.1 Å, b = 41.2 Å, c = 42.1 Å		
resolution (Å)	31.6−1.3				29.5−1.3		
no. of unique reflections.	27821	27537	27636	26499	13620	13422	13477
multiplicity	4.6	8.5	6.0	4.2	4.4	4.1	4.4
completeness (%)	95.3 (85.9)	94.7 (84.1)	94.4 (84.0)	90.0 (75.6)	84.2 (69.5)	82.5 (67.6)	82.8 (62.8)
completeness, anom (%)	94.7 (84.9)	93.6 (82.6)	93.5 (82.4)	89.2 (74.1)	82.6 (68.1)	79.9 (66.0)	81.3 (66.4)
R_{sym} (%)	9.1 (35.3)	9.2 (33.0)	9.0 (30.0)	7.6 (20.5)	7.2 (115)	6.5 (98.5)	6.8 (110)
R_{anom} (%)	7.0 (22.7)	10.6 (23.6)	6.1 (18.6)	4.2 (13.1)	5.8 (88.2)	8.2 (69.8)	5.0 (77.5)
$\langle I\rangle/\sigma(I)$	11.8 (5.5)	17.7 (9.3)	13.0 (6.6)	12.7 (7.1)	7.9 (1.4)	8.6 (1.8)	8.7 (1.6)
Wilson B (Å^2)	9.8	9.9	9.7	9.5	17.4	18.2	17.9
Cullis R, iso	0.51	0.62	−	0.47	−	0.88	0.77
Cullis R, ano	0.72	0.48	0.70	0.98	0.86	0.68	0.83
isomorphous phasing power	2.55	1.72	−	2.82	−	0.69	1.20
figure of merit (Mlphare/Dm)	0.82/0.89				0.47/0.83		

[a] Values in parentheses indicate the statistics for the 1.37−1.30 Å resolution shell. Unique reflections include Friedel mates.

Table 2: High-Resolution Data Collection Statistics[a]

	Leu12SeMet	Leu13SeMet	wild-type
λ (Å)	0.97957	1.00	1.00
space group	$P2_1$	$P2_12_12$	$P2_1$
unit cell	a = 31.2 Å, b = 47.9 Å, c = 40.5 Å, β = 93.6°	a = 37.1 Å, b = 41.2 Å, c = 42.1 Å	a = 40.6 Å, b = 37.3 Å, c = 41.2 Å, β = 90.0°
resolution (Å)	30.88−1.0	29.50−1.05	20.6−1.22
highest-resolution shell	1.05−1.0	1.11−1.05	1.29−1.22
no. of unique reflections	55221	31540	36802
multiplicity	2.8	4.3	5.3
completeness (%)	86.4 (73.1)	93.0 (82.1)	99.8 (100)
R_{sym} (%)	4.9 (10.1)	6.6 (39.8)	5.2 (49.7)
mosaicity (deg)	0.4	0.3	0.5
$\langle I\rangle/\sigma(I)$	16.8 (9.2)	16.2 (2.2)	15.9 (2.1)
Wilson B (Å^2)	7.4	10.3	16.5

[a] Values in parentheses indicate the statistics for the highest-resolution shell.

RESULTS

The general approaches for estimating initial phases in protein crystallography require incorporation of one or more ordered heavy atoms into the crystal. With the advent of multiwavelength anomalous diffraction (MAD) analysis, biosynthetic incorporation of selenomethionine has become a powerful approach to obtaining a suitable heavy atom derivative. Derivatizing a synthetic peptide crystal presents added challenges because the sequences are chemically limited, crystals can be tightly packed, and the activated selenomethionine monomer is not available commercially. To incorporate selenomethionine into a synthetic peptide, we developed a simple synthesis for Fmoc-SeMet, which was coupled in a standard peptide synthesizer.

Wild-type HNF-p1 contains methionine only at the N-terminus. Because protein termini are commonly disordered, the leucine residues at positions 12 and 13 were replaced individually with SeMet. This strategy was encouraged by studies of T4 lysozyme showing that core residues can be replaced with methionine with little structural change (*38*). The structures of both the Leu12SeMet mutant peptide (space group $P2_1$) and the Leu13SeMet mutant peptide (space group $P2_12_12$) were determined by MAD phasing (Table 1 and Figure 1). X-ray data were collected from the Leu12SeMet, Leu13SeMet, and wild-type HNF-p1 variants to 1.0, 1.1, and 1.2 Å resolution, respectively (Table 2). The model of the Leu12SeMet mutant structure was used to determine the wild-type peptide structure by molecular replacement. Crystallographic refinement of the three structures (Table 3)

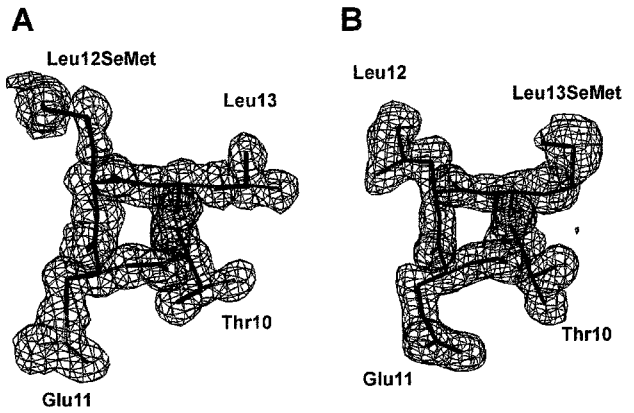

FIGURE 1: (A) Experimental electron density map of the Leu12SeMet HNF-p1 mutant at 1.0 Å resolution. The electron density (contoured at 1σ) was calculated with MAD phases after solvent flattening. The refined model is superimposed on the map. (B) Refined model of the Leu13SeMet HNF-p1 mutant superimposed on the experimental, MAD-phased electron density map at 1.3 Å resolution (contoured at 1σ).

Table 3: Refinement Statistics

	Leu12SeMet	Leu13SeMet	wild-type
no. of reflections in R_{free} set	5640 (9%)	1443 (5%)	2208 (6%)
R/R_{free} (%)	19.5/19.8	22.3/25.3	25.4/27.4
no. of non-hydrogen protein atoms	864	462	850
no. of water molecules	175	100	169
deviations from ideality			
rmsd for bond lengths (Å)	0.017	0.013	0.013
rmsd for bond angles (deg)	1.75	1.74	1.70
$\langle B\rangle$ for main chain atoms (Å^2)	12.6	11.5	19.8
$\langle B\rangle$ for side chain atoms (Å^2)	18.8	24.6	25.7
$\langle B\rangle$ for water molecules (Å^2)	26.6	31.2	33.7
φ/ψ angles			
most favored region (%)	99.1	96.4	99.0
additional allowed regions (%)	0.9	3.6	1.0
generously allowed regions (%)	–	–	–

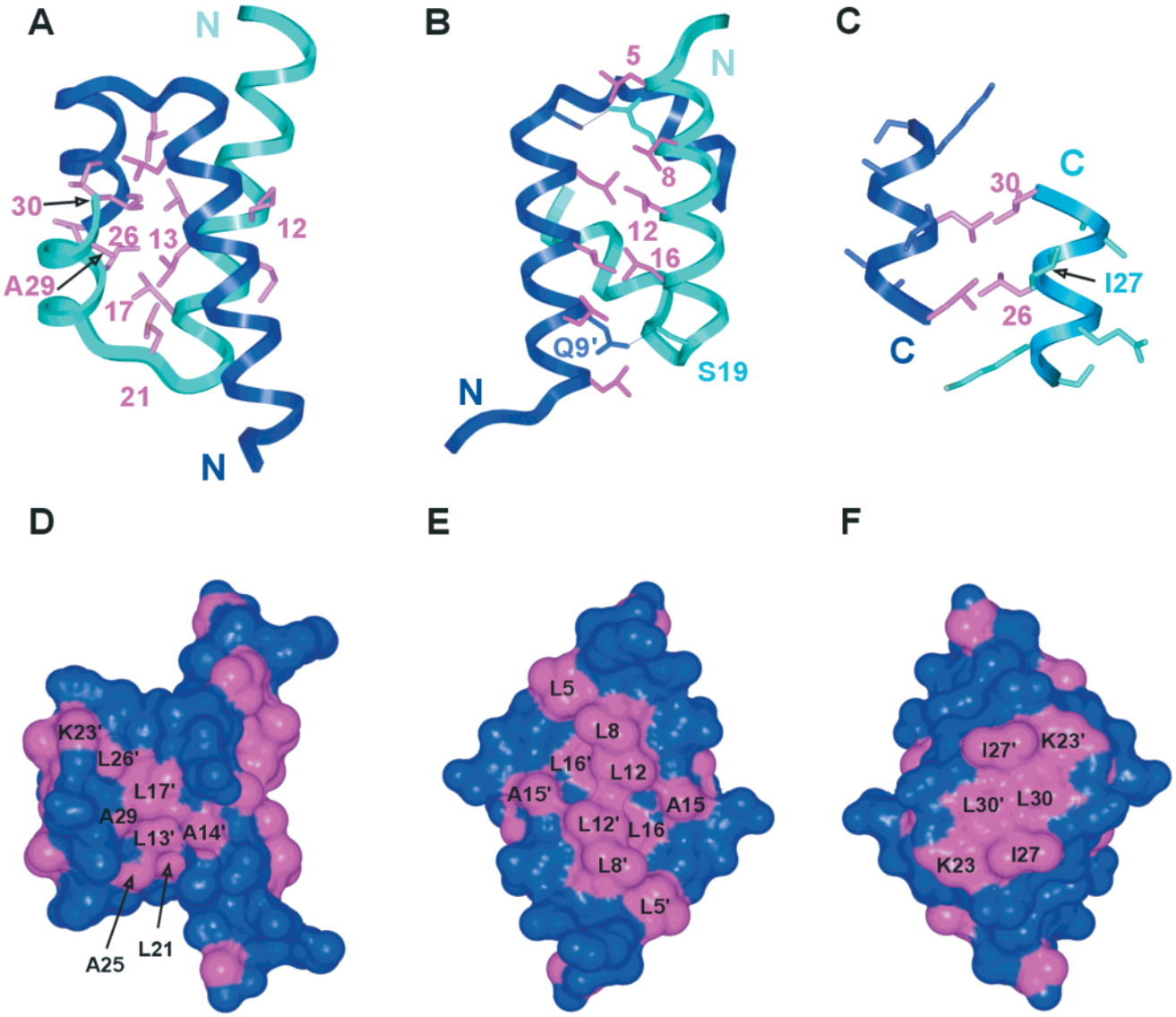

FIGURE 2: Dimerization domain of HNF-1α forms an X-type four-helix bundle. Ribbon representations with one monomer colored cyan and the other colored blue. (A) Dimer with the 2-fold rotation axis horizontal. Five leucine side chains (Leu13, Leu17, Leu21, Leu26, and Leu30) and Ala29 (magenta) form the hydrophobic core of the dimer. The positions of the two residues (Leu12 and Leu13) mutated to SeMet are labeled on one monomer. The crossing angle between the N-terminal helices is 150° and between the N- and C-terminal helices is 136−146°. (B) View along the dimer 2-fold rotation axis. Four leucine side chains (Leu5, Leu8, Leu12, and Leu16, magenta) from the N-terminal helices make hydrophobic contacts between the helices and a hydrophobic stripe on the domain surface. The side chains of Ser19 and Gln9′ are within hydrogen bonding distance at either end of the helix 1 pair. (C) Helix 2 interactions mediated by two leucine side chains (Leu26 and Leu30, magenta). (D−F) Connolly surfaces of HNF-p1 (hydrophobic side chains colored magenta and the other atoms colored blue), oriented as in panels A−C, respectively. (D) One exposed hydrophobic patch (441 Å^2) includes atoms of core leucine residues. (E) The largest hydrophobic patch (895 Å^2) on the domain surface includes the surface leucine residues of helix 1. This interface mediates DCoH recognition. (F) Hydrophobic patch (377 Å^2) on the domain surface from side chains of helix 2. This representation depicts helix 2 in the context of the complete domain.

revealed four independent copies of the Leu12SeMet mutant, two independent copies of the Leu13SeMet mutant, and four independent copies of wild-type HNF-p1.

The HNF-p1 dimer folds into an X-type (*39*), antiparallel, four-helix bundle (Figure 2). No structural homologues of the dimer were identified in the Protein Data Bank (*40*). Each monomer consists of two helices: a longer N-terminal helix (residues 4−18) and a shorter C-terminal helix (residues 22−30), connected by a short loop (residues 19−22). Helix 1 is terminated by Gly20 followed by the hydrophobic residue Leu21, forming a classic Schellman motif (*41*).

Nine of the 32 amino acids of HNF-p1 are leucine. Five of these leucines (Leu13 and Leu17 from helix 1, Leu21 from the loop, and Leu26 and Leu30 from helix 2) pack into the hydrophobic core of the dimer (Figure 2A). Leu5, Leu12, and Leu16 pack between the two N-terminal helices (Figure 2B). Leu8 is solvent-exposed. Gln9 and Ser19′ (where the prime denotes residues from the dimer-associated monomer) are positioned to form two hydrogen bonds. Leu26 and Leu30 make van der Waals contacts between C-terminal helices (Figure 2C).

Fourteen of the HNF-p1 residues are hydrophobic, and three distinct hydrophobic patches exist on the domain surface (Figure 2D−F). In all three crystal forms, the largest patch (Figure 2E, 895 Å^2), located on the helix 1 pairs, interacts with the same face on an adjacent dimer (Figure 3).

The angle between the N- and C-terminal helices differs slightly between independently refined monomers within an

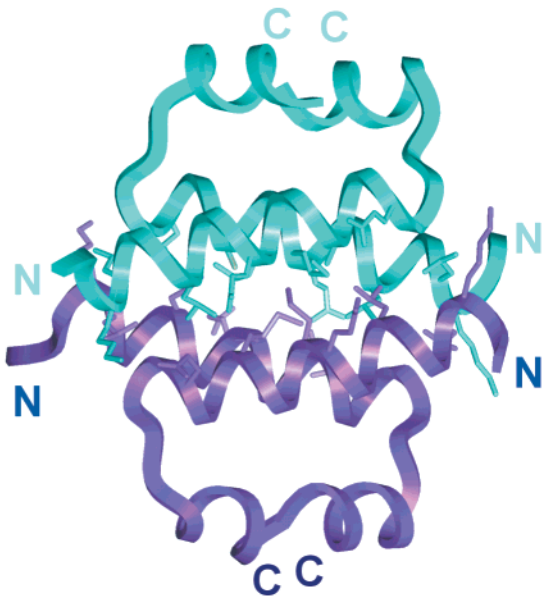

FIGURE 3: Pairing of dimers (cyan and purple ribbons) in the crystals of HNF-p1. The hydrophobic side chains that pack between the dimers are shown in a stick representation. This interaction is unstable in solution, where HNF-p1 forms a dimer at a protein concentration of ≤2 mM. The surface of helix 1 that mediates this interaction in the crystals forms the binding site for the coactivator, DCoH.

asymmetric unit, and between the wild-type and Leu12SeMet mutant proteins (Figure 4). Of the two dimers in the asymmetric unit of wild-type HNF-p1, the monomers within each dimer are virtually identical. The C-terminal helices of one of the HNF-p1 dimers are less well ordered, as evidenced by *B*-factors that are higher than those of the remainder of the protein (average of 34 Å^2 vs 18 Å^2 for backbone atoms) and breaks in the electron density. Comparisons in this paper are made with the better-ordered wild-type dimer.

The Leu13SeMet substitution is located within the dimer core. Nonetheless, the helices are oriented similarly in the Leu13SeMet and wild-type dimers (Cα rms deviation = 0.25 Å). The two independent Leu13SeMet monomers are virtually identical (Cα rms deviation = 0.14 Å for residues 4−32). In contrast, the four independent Leu12SeMet monomers show variability in the interhelical angle (Cα rms deviation = 1.2−2.0 Å for residues 4−32) that leads to small differences from the wild-type conformation (Cα rms deviation = 0.7−1.4 Å). This observation was confirmed by the finding that applying noncrystallographic symmetry restraints to the four Leu12SeMet chains increased the R and R_{free} values to greater than 40%. Leu12 is located on the surface of the N-terminal helix away from the dimer core, not in contact with helix 2 (Figure 2A). For each of the HNF-p1 monomer orientations, the loop residues (Ser19, Gly20, Leu21, and Ser22) shift to accommodate changes in helix packing, while the individual helices are extremely similar (Cα rms deviation for helix 1 = 0.20−0.26 Å, Cα rms deviation for helix 2 = 0.26−0.29 Å).

DISCUSSION

The homeodomain DNA-binding motif of HNF-1 is shared by more than 100 distinct proteins in humans. Homeodomain proteins play essential roles in transcriptional regulation during development and cellular differentiation. Paradoxically, isolated homeodomains from transcription factors with distinct biological functions bind similar DNA sequences (reviewed in ref *42*). In some cases, sequence selectivity is enhanced by cooperative binding of two homeodomain proteins (*43*−*49*). Alternatively, a number of homeodomain proteins contain distinct dimerization domains that promote pairing in solution. From a biological perspective, dimerization allows the selection of a protein partner prior to DNA binding and enables the formation of dominant negative heterodimers that do not bind DNA (*1*). HNF-1 proteins are among the few dimeric homeodomain proteins in the animal kingdom. Other dimeric homeodomain proteins include Mat a1/α2 in yeast (*50*) and a family of leucine−zipper homeodomain proteins in plants (*51*).

The structure reported here demonstrates that the dimerization domain of HNF-1α forms an X-type, four-helix

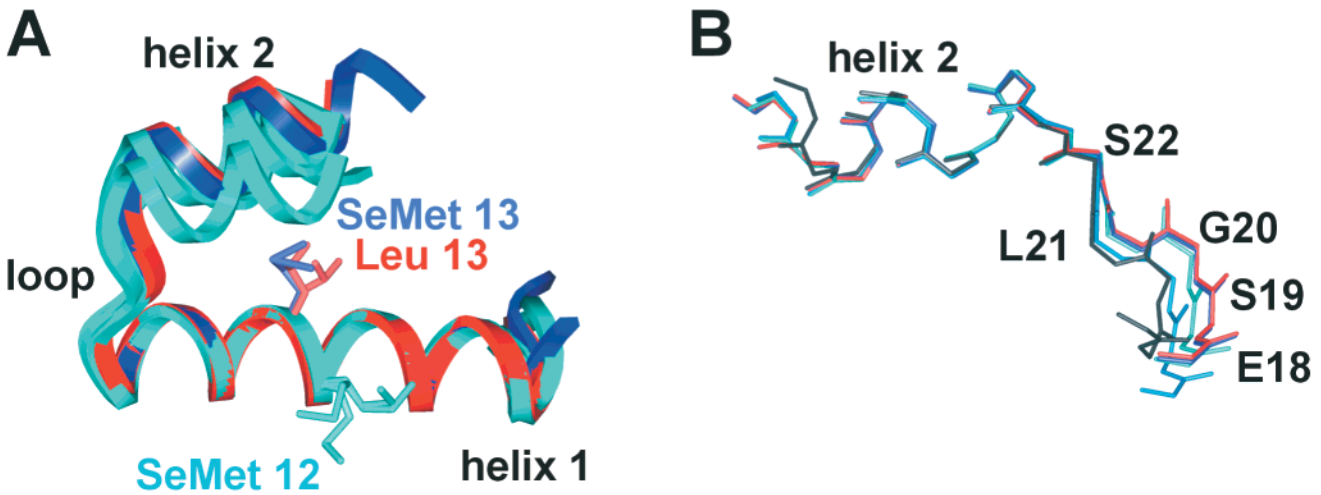

FIGURE 4: Small variations in the angle between the N- and C-terminal helices of HNF-p1 wild-type monomers and the Leu-to-SeMet mutants. (A) Ribbon diagram of eight independently refined monomers superimposed using the Cα atoms of helix 1. Two monomers of the wild-type structure (red) and the two monomers from the Leu13SeMet structure (blue) are closely similar. Helix 2 of the four monomers from the Leu12SeMet structure (cyan) adopts four slightly different orientations. The four SeMet12 (cyan), two SeMet13 (blue), and two wild-type Leu13 (red) rotamers are displayed. (B) Backbone atoms of eight independently refined monomers overlapped via the Cα atoms of helix 2. Small changes in the main chain dihedral angles of loop residues (Ser19, Gly20, Leu21, and Ser22) coincide with variations in the interhelical angle. Atoms are colored as in panel A.

bundle. X-type four-helix bundles with different folds exist in several multimer interfaces (*52*). The cAMP-dependent protein kinase (PKA) (*53*) contains an antiparallel four-helix bundle dimerization domain, similar to the dimerization domains of calcyclin (*54*) and the calcium-bound form of S100B($\beta\beta$) (*55*). Like HNF-p1, the dimerization domains of both PKA and S100B($\beta\beta$) also function as interfaces for heterologous proteins, binding A kinase-anchoring proteins and p53, respectively.

Dimerization interfaces also are formed by pairs of helical hairpins, for example, the antiparallel hairpins in CheA (*56*) and ColE1 Rop (*57*) and the parallel hairpins in SpoA (*58*). Structures of autonomous, tetrameric four-helix bundle interfaces include Mnt repressor (*59*), p53 (*60*), and lac repressor (*61*). These examples demonstrate the diversity among four-helix bundle dimerization and tetramerization domains. Compared to HNF-p1, these bundles display different crossing angles, helical lengths, and packing interactions.

A Distinct Dimerization Motif. The structure of the HNF-1α dimerization domain was determined by incorporating selenomethionine into mutant synthetic peptides for MAD phasing. Synthesis of SeMet-containing peptides was facilitated by developing a simple protocol for synthesis of Fmoc-SeMet from readily purchased precursors. Singly substituted peptides at consecutive Leu residues were synthesized. Leu12SeMet is located on the domain surface, and Leu13SeMet is located in the domain core. Both SeMet substitutions produced different, highly ordered crystals. This strategy may be generally useful for determining crystal structures of synthetic peptides and proteins.

Crystal structures of HNF-p1, both alone and in complex with DCoH (*25*), define a dimerization motif with no structural homologues. On the basis of sequence homology with myosin, HNF-p1 was initially predicted to form a coiled coil (*5*). Sequence features that may specify the distinct HNF-p1 fold include leucine residues that pack in the core at positions 13, 16, 17, 21, 26, and 30; the Ser-Gly-Leu sequence that forms the flexible loop terminating helix 1; two hydrogen bonds between the N-terminal helices; and the uneven lengths of the helices in each monomer.

The crystal structures provide evidence for flexibility in the C-terminal helix of HNF-p1. The wild-type HNF-p1 crystals contain two independent dimers with different angles between helix 1 and helix 2 (Figure 4), and the C-terminal helices are less ordered in one of the dimers. The Leu13SeMet substitution appears to stabilize the domain structure, since these crystals contain only one conformation that is identical to the well-ordered, wild-type monomer. The structure of the Leu12SeMet-substituted peptide contains four distinct angles between helix 1 and helix 2 that also differ from the wild-type conformation (Figure 4). These small shifts may reflect the effects of differences in the crystal contacts of helix 2 in all three crystal forms.

HNF-1α and HNF-1β dimers readily exchange (in the absence of DCoH) to form heterodimers (*11*). Nine residues differ between the dimerization domains of HNF-1α and HNF-1β (Figure 5). Eight of these residues occupy solvent-exposed positions in the HNF-p1 structure. The conservative substitution of Val21 in HNF-1β for Leu21 in HNF-1α is located in a buried position in the loop. The overall conservation of the interfacial residues between the monomers is consistent with heterodimer formation.

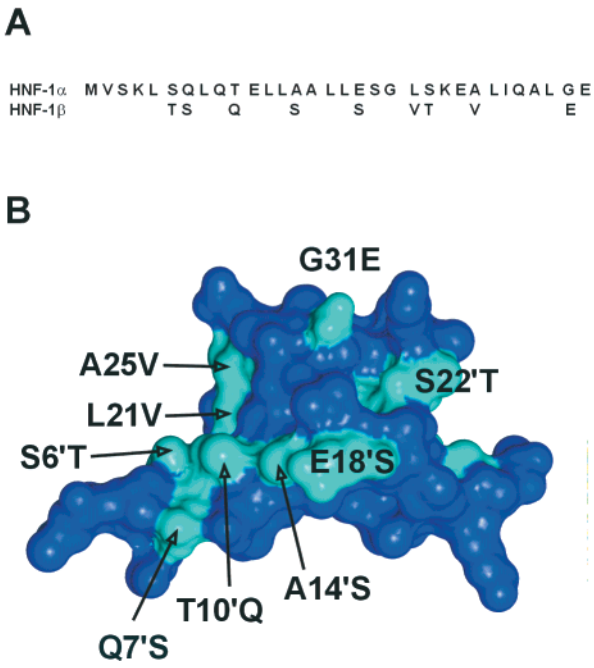

FIGURE 5: Sequence differences between the dimerization domains of HNF-1α and HNF-1β are confined largely to surface residues. (A) Sequence of the HNF-1α dimerization domain and the changes in the corresponding region of HNF-1β. (B) Connolly surface of HNF-p1 indicating the locations of the nine amino acid differences (cyan) between the dimerization domains of HNF-1α and HNF-1β. Labels indicate the substitutions in HNF-1β. Eight of the nine amino acid differences are situated on the surface of the domain. A conservative substitution in the core, Leu21Val, occurs at a site that makes no contacts across the dimer interface.

Comparison with the Solution Structure. NMR measurements indicated that HNF-p1 contains two helices (residues 7−18 and 23−32) (*27*). The secondary structure of HNF-p1 in the crystal structure agrees with the NMR determination except for residues 4−7, which are helical in the crystal structure. The lack of long-range NOEs initially prevented the direct determination of the tertiary structure in solution and supported the prediction that HNF-p1 forms a parallel, four-helix bundle (*27*, *28*). In contrast, a recent report, based on a detailed, three-dimensional structure of unlabeled peptide determined by NMR (*26*), suggested that HNF-p1 forms an antiparallel four-helix bundle containing helical hairpins (Figure 6A).

The tertiary fold in this solution structure differs markedly from the crystal structure of HNF-p1 reported here. In the solution structure, the two helices within each monomer are antiparallel, and they make extensive contacts with each other. In contrast, the monomers in the crystal structure form a V shape with limited interhelical contacts (Figure 6B). Interactions between monomers in the dimer stabilize the V-shaped fold in the crystals (Figure 2A). In addition, the monomers in the solution structure pack along different faces of the helices than in the crystal structure (Figure 6C). This difference in packing causes different residues to be situated in the protein core. As a result, the surface residues that form the continuous interface with DCoH in the DCoH−HNF-p1 complex (*25*) are dispersed in the solution structure of the HNF-p1 dimer. In contrast, no gross conformational rearrangements in the HNF-p1 crystal structure are required to form the DCoH binding surface (Figure 7).

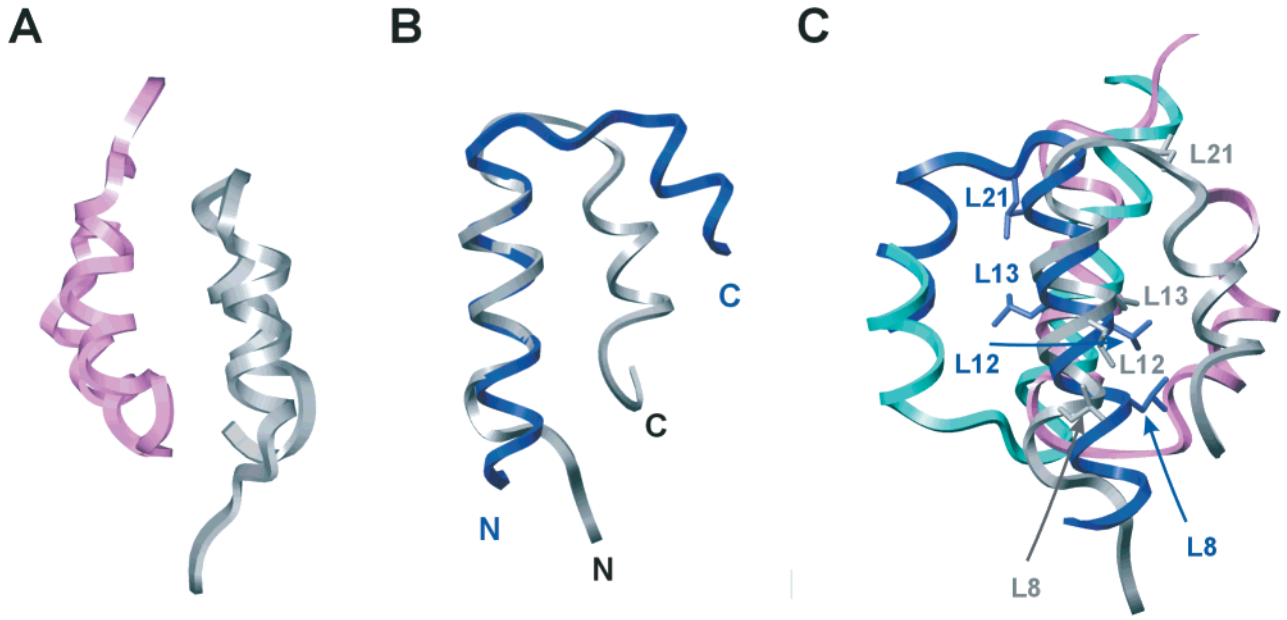

FIGURE 6: Comparison of the NMR and crystal structures of HNF-p1. (A) Ribbon diagram of the NMR structure (PDB entry 1dt8) of the HNF-p1 dimer (*26*). The solution structure comprises a dimer of antiparallel helical hairpins. In contrast, an X-type, four-helix bundle was observed in the crystal structure (compare to Figure 2B). (B) Large differences between the solution and crystal structures of the HNF-p1 monomers. Helix 1 (Cα atoms of residues 8−18) of the solution (gray) and crystal (blue) structures were superimposed (rms deviation = 0.86 Å) using monomer 2 of the solution structure (PDB entry 1dt8). Unlike the antiparallel helices in the solution structure, the helices in the crystal structure form a larger acute angle. In the best overall superposition of the monomers (not shown), the rms deviation of the Cα atoms of residues 8−30 was greater than 3.4 Å. (C) Superposition of the NMR (gray and pink) and crystal (blue and cyan) structures of the HNF-p1 dimer. The helix 1 pairs (Cα atoms of residues 8−18 of both monomers) were superimposed with an rms deviation of 4.3 Å. The superposition reveals that the axial rotation of helix 1 differs in the solution and crystal structures. In the NMR structure, a different face of helix 1 forms the dimer interface and helix 2 occurs on the other side of helix 1 compared to the crystal structure. As a result, different residues make up the buried core in the two structures. Amino acids on the surface of helix 1 positioned to contact DCoH also differ in the solution and crystal structures. The rms deviation of the dimers superimposed using the Cα atoms of residues 8−30 (not shown) was 8.4 Å.

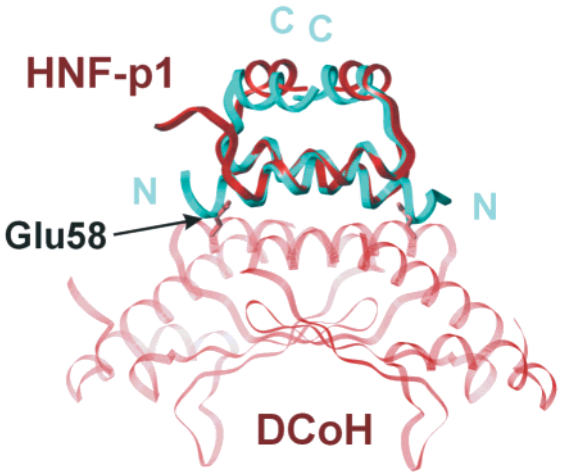

FIGURE 7: Structural changes in HNF-p1 promoted by DCoH binding. Superposition of the isolated HNF-p1 dimer (cyan) and HNF-p1 in the HNF-p1−DCoH complex (brown) (*25*) based on the Cα atoms of residues 8−18. Helix 1 in free HNF-p1 is one turn longer than the equivalent helix in the DCoH complex. In the complex, DCoH Glu58 caps the N-terminus of HNF-p1 helix 1 at residue 8, blocking extension of the helix toward the HNF-p1 N-terminus. Shifts also are evident in helix 2.

Determination of the tertiary structure of HNF-p1 by NMR has been impeded by the flexibility and 2-fold symmetry of the dimer and the paucity of long-range NOEs (*27*, *28*). For each 33-residue monomer in the recently determined NMR structure (*26*), 34 long-range, intramonomer NOEs and 20 intermonomer NOEs were identified (PDB entry 1dt8). The assigned intermonomer NOEs between Gln9 and Ser19′ and between Gln9 and Leu21′ generally agree with the crystal structure, reflecting contacts between the N- and C-termini of helix 1 in both structures.

A large fraction of the long-range and intermonomer NOEs, however, are inconsistent with the crystal structure. Of the 34 long-range, intramonomer NOEs, 20 were assigned to contacts with Trp33, a mutant residue that was added to the C-terminus of the HNF-p1 sequence for the solution work. (This Trp residue was absent from the peptides used in the crystallographic studies.) Thirteen of the remaining 14 long-range, intramonomer NOEs are incompatible with the crystal structure (i.e., interproton distances >6.4 Å). In addition, six NOEs attributed to intermonomer contacts in solution were assigned to protons that are expected to be >6 Å apart in the crystal structure. For Leu5 and Leu21′, the increased distances in the crystal structure (6.7−11 Å) reflect the extension of the N-terminal helix that may result from interdimer crystal contacts.

The fold observed in the crystal structure was preserved in five independent dimers formed by three HNF-p1 sequence variants in three different crystal forms. Similar peptide concentrations were used for the NMR [2 mM (*26*)] and crystallographic (1.5 mM) studies. Thus, barring a global conformational rearrangement upon crystallization or perturbation of the structure by the non-native Trp residue added to the C-terminus for the solution work, it is possible that the NMR structure may require revision.

Comparison with the HNF-p1−DCoH Complex. With local conformational changes, the overall fold of HNF-p1

is conserved in the structure of the HNF-p1−DCoH complex (*25*). DCoH stabilizes the HNF-1 dimer (*16*) by binding the N-terminal helices of HNF-p1 (*25*). Superimposing the N-terminal helices of complexed and unbound HNF-p1 reveals shifts in the HNF-p1 C-terminal helices, alternative rotamers for several residues in helix 1, and changes in the conformation of residues 1−7 (Figure 7). DCoH Glu58 caps the N-terminus of HNF-p1 helix 1 at residue 8, stabilizing the shorter helix 1 (*25*). In contrast, helix 1 includes residues 4−7 in the crystal structure of the isolated HNF-p1. These variations in the first helical turn of HNF-p1 may facilitate protein binding and modulate the stability of the coactivator complex. Similar roles for conformational flexibility were proposed for the POU domain of the transcription factor, PIT-1 (*45*, *62*).

The longer helix 1 observed in the isolated HNF-p1 may be stabilized in the crystals by pairing with a second dimer through the N-terminal helices. The contacts between HNF-p1 dimers (Figure 3) bury 1790 Å^2 of helix 1 (895 Å^2 from each monomer), similar to the 1866 Å^2 surface area buried in the HNF-p1−DCoH complex. Although the HNF-p1 peptide is dimeric in solution at concentrations up to 1−2 mM (*26*, *63*), the helix 1 interactions between dimers in the crystals may have biological relevance. In support of this idea, the contacts between helix 1 pairs, but not helix 2 pairs, are conserved in the three crystal forms of HNF-p1 variants. A number of promoters, including the promoters for the human insulin-like growth factor 1 (*64*) and the α-fetoprotein (*65*), contain multiple HNF-1 binding sites. The local concentration of HNF-1 bound to DNA may promote interactions of HNF-1 dimers, which in turn might stabilize the DNA-bound HNF-1. Such direct interactions of dimerization domains have been shown to induce cooperative assembly of transcription factors (such as STAT-4 and Fos/Jun) in other promoter complexes (*66*−*68*).

Three MODY3 Mutations in HNF-p1. Mutations in both HNF-1α and HNF-1*β* have been associated with MODY, an inherited form of diabetes. Three MODY3 mutations are located in the HNF-1α dimerization domain: Leu12His (*69*), Gly20Arg (*70*), and Gly31Asp (*71*). We previously demonstrated that the Leu12His and Gly20Arg mutations disrupt DNA binding and DCoH binding to HNF-1α (*25*). The HNF-p1 crystal structure is consistent with the observation that these MODY3 mutations disrupt dimer formation (*25*, *26*). Leu12 is substantially buried, and Gly20 forms a critical element of the Schellman motif that forms the terminus of helix 1. The third MODY3 mutation, Gly31Asp, preserves dimerization and DNA binding (*25*). Gly31 was not well-resolved in the HNF-p1−DCoH complex structure. The structure presented here indicates that Gly31 borders a hydrophobic patch on the surface of the C-terminal helices (Figure 2F). The location of Gly31 on the periphery of the dimerization domain structure supports the idea that this surface may interact with another segment of HNF-1 or with an unknown factor. Interestingly, an acidic residue, Glu, occurs at position 31 in HNF-1*β*. Consequently, the Gly31Asp substitution may modulate the activity of dimers containing mutant HNF-1α chains in a manner analogous to Glu31 in HNF-1*β*. The central (Leu12 and Gly20) and peripheral (Gly31) locations of the MODY3 mutations in the HNF-p1 structure are consistent with the finding that these mutations act by distinct mechanisms (*25*).

Conclusions. HNF-1α and HNF-1*β* are the only known proteins that contain the HNF-p1 fold. This singularity restricts dimerization to HNF-1 proteins, isolating them from more prevalent dimerization partners such as leucine−zipper or bHLH proteins. The surface locations of residues that differ in HNF-1α and HNF-1*β* are consistent with homo- and heterodimerization of these proteins. The dimerization domain of HNF-1 provides a stable platform for interactions with other proteins, such as the coactivator DCoH and possibly with a neighboring HNF-1 dimer on DNA.

ACKNOWLEDGMENT

We thank Jerry Crabtree for helpful discussions and continuous encouragement. We are indebted to David S. King for peptide synthesis and mass spectrometry. Data were collected at the Advanced Light Source, Lawrence Berkeley National Laboratory. The Advanced Light Source is supported by the Director, Office of Science, Office of Basic Energy Sciences, Materials Sciences Division, of the U.S. Department of Energy under Contract DE-AC03-76SF00098 at Lawrence Berkeley National Laboratory.

REFERENCES

1. Jones, N. (1990) *Cell 61*, 9−11.
2. Nakabeppu, Y., Ryder, K., and Nathans, D. (1988) *Cell 55*, 907−915.
3. Chiu, R., Angel, P., and Karin, M. (1989) *Cell 59*, 979−986.
4. Schütte, J., Viallet, J., Nau, M., Segal, S., Fedorko, J., and Minna, J. (1989) *Cell 59*, 987−997.
5. Nicosia, A., Monaci, P., Tomei, L., De Francesco, R., Nuzzo, M., Stunnenberg, H., and Cortese, R. (1990) *Cell 61*, 1225−1236.
6. Tronche, F., and Yaniv, M. (1992) *BioEssays 14*, 579−587.
7. Mendel, D. B., and Crabtree, G. R. (1991) *J. Biol. Chem. 266*, 677−680.
8. Yamagata, K., Oda, N., Kaisaki, P. J., Menzel, S., Furuta, H., Vaxillaire, M., Southam, L., Cox, R. D., Lathrop, G. M., Boriraj, V. V., Chen, X., Cox, N. J., Oda, Y., Yano, H., Le Beau, M. M., Yamada, S., Nishigori, H., Takeda, J., Fajans, S. S., Hattersley, A. T., Iwasaki, N., Hansen, T., Pedersen, O., Polonsky, K. S., Turner, R. C., Velho, G., Chevre, J., Froguel, P., and Bell, G. I. (1996) *Nature 384*, 455−458.
9. Nishigori, H., Yamada, S., Kohama, T., Tomura, H., Sho, K., Horikawa, Y., Bell, G. I., Takeuchi, T., and Takeda, J. (1998) *Diabetes 47*, 1354−1355.
10. Horikawa, Y., Iwasaki, N., Hara, M., Furuta, H., Hinokio, Y., Cockburn, B. N., Lidner, T., Yamagata, K., Ogata, M., Tomonaga, O., Kuroki, H., Kasahara, T., Iwamoto, Y., and Bell, G. I. (1997) *Nat. Genet. 17*, 384−385.
11. Mendel, D. B., Hansen, L. P., Graves, M. K., Conley, P. B., and Crabtree, G. R. (1991) *Genes Dev. 5*, 1042−1056.
12. Rey-Campos, J., Chouard, T., Yaniv, M., and Cereghini, S. (1991) *EMBO J. 10*, 1445−1457.
13. Lazzaro, D., De Simone, V., De Magistris, L., Lehtonen, E., and Cortese, R. (1992) *Development 114*, 469−479.
14. De Simone, V., De Magistris, L., Lazzaro, D., Gerstner, J., Monaci, P., Nicosia, A., and Cortese, R. (1991) *EMBO J. 10*, 1435−1443.
15. De Francesco, R., Pastore, A., Vecchio, G., and Cortese, R. (1991) *Biochemistry 30*, 143−147.
16. Mendel, D. B., Khavari, P. A., Conley, P. B., Graves, M. K., Hansen, L. P., Admon, A., and Crabtree, G. R. (1991) *Science 254*, 1762−1767.
17. Baumhueter, S., Courtois, G., and Crabtree, G. R. (1988) *EMBO J. 7*, 2485−2493.
18. Cereghini, S., Blumenfeld, M., and Yaniv, M. (1988) *Genes Dev. 8*, 957−974.
19. Olsen, J., Classen-Linke, I., Sjöström, H., and Norén, O. (1995) *Biochem. J. 312*, 31−37.

20. Bach, I., and Yaniv, M. (1993) *EMBO J. 12*, 4229−4242.
21. Ott, M. O., Rey-Campos, J., Cereghini, S., and Yaniv, M. (1991) *Mech. Dev. 36*, 47−58.
22. Blumenfeld, M., Maury, M., Chouard, T., Yaniv, M., and Condamine, H. (1991) *Development 113*, 589−599.
23. Cereghini, S., Ott, M.-O., Power, S., and Maury, M. (1992) *Development 116*, 783−797.
24. Wang, W., Hayashi, Y., Ninomiya, T., Ohta, K., Nakabayashi, H., Tamaoki, T., and Itoh, H. (1998) *J. Pathol. 184*, 272−278.
25. Rose, R. B., Bayle, J. H., Endrizzi, J. A., Cronk, J. D., Crabtree, G. R., and Alber, T. (2000) *Nat. Struct. Biol. 7*, 744−748.
26. Hua, Q., Zhao, M., Narayana, N., Nakagawa, S. H., Jia, W., and Weiss, M. A. (2000) *Proc. Natl. Acad. Sci. U.S.A. 97*, 1999−2004.
27. Pastore, A., De Francesco, R., Barbato, G., Morelli, M. A. C., Motta, A., and Cortese, R. (1991) *Biochemistry 30*, 148−153.
28. Pastore, A., De Francesco, R., Morelli, M. A. C., Nalis, D., and Cortese, R. (1992) *Protein Eng. 5*, 749−757.
29. Leslie, A. G. W., Brick, P., and Wonacott, A. (1986) *Daresbury Laboratory Information Quarterly for Protein Crystallography*, Vol. 18, pp 33−39, Daresbury Laboratory, Warrington, U.K.
30. Evans, P. R. (1993) Data reduction, in *Proceedings of CCP4 Study Weekend on Data Collection & Processing*, Daresbury Laboratory, Warrington, U.K.
31. Terwilliger, T. C., and Berendzen, J. (1999) *Acta Crystallogr. D55*, 849−861.
32. Collaborative Computing Project No. 4 (1994) *Acta Crystallogr. D50*, 760−763.
33. Cowtan, K. (1994) in *Joint CCP4 and ESF-EACBM Newsletter on Protein Crystallography*, Daresbury Laboratory, Warrington, U.K.
34. Perrakis, A., Morris, R., and Lamzin, V. S. (1999) *Nat. Struct. Biol. 6*, 458−463.
35. Jones, T. A., Zhou, J. Y., Cowan, S. W., and Kjeldgaard, M. (1991) *Acta Crystallogr. A47*, 110−119.
36. Tronrud, D. E. (1992) *Acta Crystallogr. A48*, 912−916.
37. Brünger, A. T., Adams, P. D., Clore, G. M., DeLano, W. L., Gros, P., Grosse-Kunstleve, R. W., Jiang, J. S., Kuszewski, J., Nilges, M., Pannu, N. S., Read, R. J., Rice, L. M., Simonson, T., and Warren, G. L. (1998) *Acta Crystallogr. D54*, 905−921.
38. Gassner, N. C., Baase, W. A., and Matthews, B. W. (1996) *Proc. Natl. Acad. Sci. U.S.A. 93*, 12155−12158.
39. Harris, N. L., Presnell, S. R., and Cohen, R. E. (1994) *J. Mol. Biol. 236*, 1356−1368.
40. Holm, L., and Sander, C. (1993) *J. Mol. Biol. 233*, 123−138.
41. Aurora, R., Srinivasan, R., and Rose, G. D. (1994) *Science 264*, 1126−1130.
42. Gehring, W. J., Qian, Y. Q., Billeter, M., Furukubo-Tokunaga, K., Schier, A. F., Resendez-Perez, D., Affolter, M., Otting, G., and Wüthrich, K. (1994) *Cell 78*, 211−223.
43. White, R. (1994) *Curr. Biol. 4*, 48−50.
44. Wilson, D. S., and Desplan, C. (1995) *Curr. Biol. 5*, 32−34.
45. Jacobson, E. M., Li, P., Leon-del-Rio, A., Rosenfeld, M. G., and Aggarwal, A. K. (1997) *Genes Dev. 11*, 198−212.
46. Tan, S., and Richmond, T. J. (1998) *Nature 39*, 660−666.
47. Wilson, D. S., Guenther, B., Desplan, C., and Kuriyan, J. (1995) *Cell 82*, 709−719.
48. Passner, J. M., Ryoo, H. D., Shen, L., Mann, R. S., and Aggarwal, A. K. (1999) *Nature 397*, 714−719.
49. Li, T., Stark, M. R., Johnson, A. D., and Wolberger, C. (1995) *Science 270*, 262−269.
50. Ho, C., Adamson, J. G., Hodges, R. S., and Smith, M. (1994) *EMBO J. 13*, 1403−1413.
51. Chan, R. L., Gago, G. M., Palena, C. M., and Gonzalez, D. H. (1998) *Biochim. Biophys. Acta 1442*, 1−19.
52. Lin, S. L., Tsai, C. J., and Nussinov, R. (1995) *J. Mol. Biol. 248*, 151−161.
53. Newlon, M. G., Roy, M., Morikis, D., Hausken, Z. E., Coghlan, V., Scott, J. D., and Jennings, P. A. (1999) *Nat. Struct. Biol. 6*, 222−227.
54. Potts, B. C., Smith, J., Akke, M., Macke, T. J., Okazaki, K., Hidaka, H., Case, D. A., and Chazin, W. J. (1995) *Nat. Struct. Biol. 2*, 790−796.
55. Drohat, A. C., Baldisseri, D. M., Rustandi, R. R., and Weber, D. J. (1998) *Biochemistry 37*, 2729−2740.
56. Bilwes, A. M., Alex, L. A., Crane, B. R., and Simon, M. I. (1999) *Cell 96*, 131−141.
57. Banner, D. W., Kokkinidis, M., and Tsernoglou, D. (1987) *J. Mol. Biol. 196*, 657−675.
58. Varughese, K. I., Madhusudan, Zhou, X. Z., Whiteley, J. M., and Hoch, J. A. (1998) *Mol. Cell 2*, 485−493.
59. Nooren, I. M. A., Kaptein, R., Sauer, R. T., and Boelens, R. (1999) *Nat. Struct. Biol. 6*, 755−759.
60. Jeffrey, P. D., Gorina, S., and Pavletich, N. P. (1995) *Science 267*, 1498−1501.
61. Friedman, A. M., Fischmann, T. O., and Steitz, T. A. (1995) *Science 268*, 1721−1727.
62. Ryan, A. K., and Rosenfeld, M. G. (1997) *Genes Dev. 11*, 1207−1225.
63. Cronk, J. D. (1996) Structural studies of DCoH, a bifunctional enzyme and protein-binding transcriptional coactivator, Ph.D. Dissertation, University of California, Berkeley, CA.
64. Nolten, L. A., Steenbergh, P. H., and Sussenbach, J. S. (1995) *Mol. Endocrinol. 9*, 1488−1499.
65. Sawadaishi, K., Morinaga, T., and Tamaoki, T. (1988) *Mol. Cell. Biol. 8*, 5179−5187.
66. Carey, M. (1998) *Cell 92*, 5−8.
67. Chen, L., Glover, J. N. M., Hogan, P. G., Rao, A., and Harrison, S. C. (1998) *Nature 392*, 42−48.
68. Vinkemeier, U., Moarefi, I., Darnell, J. E. J., and Kuriyan, J. (1998) *Science 279*, 1048−1052.
69. Iwasaki, N., Oda, N., Ogata, M., Hara, M., Hinokio, Y., Oda, Y., Yamagata, K., Kanematsu, S., Ohgawara, H., Omori, Y., and Bell, G. I. (1997) *Diabetes 46*, 1504−1508.
70. Boutin, P., Chevre, J. C., Hani, E., Gomis, R., Pardini, V. C., Guillausseau, P., Vaxillaire, M., Velho, G., and Froguel, P. (1997) *Diabetes 46*, 2108−2109.
71. Maire, P., Wuarin, J., and Schibler, U. (1989) *Science 244*, 343−346.

BI001996T